Microphysics of Raindrop Size Spectra: Tropical Continental and Maritime Storms

CARLTON W. ULBRICH

Department of Physics and Astronomy, Clemson University, Clemson, South Carolina

DAVID ATLAS

Laboratory for Atmospheres, NASA Goddard Space Flight Center, Greenbelt, Maryland

(Manuscript received 9 September 2006, in final form 21 February 2007)

ABSTRACT

This work uses raindrop size spectra measured at the surface in tropical continental storms to determine the associated parameters of the best-fit gamma distributions. The physical processes responsible for those parameters and their relations to the measurable radar reflectivity Z and differential reflectivity ZDR are then explored. So too are their relations to quantitative measurements of rain. Comparison is then made with corresponding features previously reported in tropical maritime regimes. The storms observed in Brazil and Arecibo, Puerto Rico, have been divided into convective (C), transition (T), and stratiform (S) segments. The raindrop size distribution (DSD) parameters are clearly defined on a gamma parameter diagram (GPD) that shows 1) how median volume drop size D_0 increases from S to T to C segments of the rain while 2) the range of the spectrum breadth parameter μ increases, and the range of the slope parameter Λ decreases in the same sequence of S to C. Drop growth occurs predominantly below the 0°C level by collision, coalescence, and breakup in the C rains. The median volume diameter D_0 grows as more of the water is concentrated near that size and so the DSD narrows; that is, both μ and Λ increase. In both maritime and continental storms the DSD in the convective portion of the storm approaches equilibrium. The coefficient A in the $Z = AR^b$ relation increases with D_0 while the exponent b approaches unity. The D_0 and A pair increase with, and appear to be determined largely by, the updraft strength, thus providing a possible means of determining the appropriate algorithms for rainfall measurement. Although the small drop number samples measured by the surface disdrometer relative to the large volumes sampled by a radar tend to truncate the DSD at both small and large drop sizes, narrow distributions with $\mu = 5$ to 12 cannot be attributed to such an effect. Such narrow DSDs accord with common experience of monodispersed large drops at the beginning of a convective storm. There is also remarkable agreement of the surface-based observations of ZDR–Z–D_0 with the time–space variations from C to T to S rain types observed by radar in England and elsewhere. Because the C region of a storm often accounts for a major share of the rain accumulation despite its shorter duration, it is particularly important to measure that region more accurately. There are distinctive clusters of the generalized number parameter N_W versus D_0 between maritime and continental storms. Methods for remote sensing and parameterization must partition the rainstorms into convective, transition, and stratiform segments.

1. Introduction

In a prior work by Atlas and Ulbrich (2006, hereinafter AU1), we dealt with the nature of the parameters of the gamma distribution of raindrops in *maritime* tropical convective storms. In the current paper we focus on *continental* tropical convective storms and their comparison with their maritime counterparts. In particular we shall deal with drop size distributions (DSDs) observed during the Tropical Rainfall Measuring Mission Large-Scale Biosphere–Atmosphere (TRMM LBA) experiments in Rondonia, Brazil (Atlas and Williams 2003, hereinafter AW), and near Arecibo, Puerto Rico, in 1998 (Ulbrich et al. 1999). The convective storms in both places are more intense than those found in the oceanic regions and produce larger raindrops. The ultimate goal is to define the dominant properties of the drop size distribution, their microphysical origin, and their association with the physical characteristics of the storms responsible for their generation in the ex-

Corresponding author address: Dr. Carlton W. Ulbrich, 106 Highland Drive, Clemson, SC 29631.
E-mail: cwu@nctv.com

DOI: 10.1175/2007JAMC1649.1

© 2007 American Meteorological Society

pectation that one may determine a matrix of radar-rainfall algorithms matched to those physical features.

The attempt to make such a match has a long and rich history starting with Marshall and Palmer (1948), Wexler (1951), Imai et al. (1955), Atlas and Chmela (1957), Mueller (1965), Fujiwara (1965), Cataneo and Stout (1968), Tokay and Short (1996), Testud et al. (2001), and so on. All these and more are summarized in a notable comprehensive review and synthesis by Rosenfeld and Ulbrich (2003). They have shown how a variety of physical processes such as coalescence, breakup, evaporation, size sorting by drafts, and wind shear affect the DSD. They have also ordered the median volume diameters D_0 and water contents based upon DSDs and Z–R relations in 12 regions ranging from maritime to continental. What they and other investigators have omitted, however, was the fact that most of the studies on which they draw failed to partition each storm into their Z–R relations according to convective (C), transition (T), and stratiform (S) rain, so that those relations are a nonlinear combination of the various rain types. Even the work of Fujiwara (1965), which classified the storms as "continuous rain, rain showers, and thunderstorms," failed to divide the thunderstorms into their C, T, and S subsets. One of our main goals is to overcome such oversights.

Another important recent contribution is the work of Bringi et al. (2003, hereinafter BRAL). They used polarimetric radar and surface-based DSD observations to find distinct clusters of the "generalized" drop number concentration and the mean volume diameter for maritime and continental convective storms. This has led us to determine the specific features of the DSDs and the nature of the physical storm characteristics corresponding to such clusters.

Still another perceptive critical review of precipitation measurements by radar from ground and space is the paper by Chandrasekar et al. (2003). They point out the variety of practical factors that limit the use of DSD-based Z–R relations for actual rainfall measurements. Nevertheless the latter relations remain an important point of departure for understanding the physical processes. Throughout this work we also refer frequently to the exceptional book by Bringi and Chandrasekar (2001, hereinafter BC).

The instrument used in the observations reported here is the Joss–Waldvogel Disdrometer (JWD, also known as the RD-69; Joss and Waldvogel 1967). The pros and cons of the JWD and references thereto have been discussed in AU1. All the samples are of 1-min duration. The instrument dead time correction was applied to calculations performed in this work, including those described in the next section, and it was found to have only a minor effect on integral parameters calculated from the DSDs. We shall refer again to the limitations of small samples observed by the JWD relative to the very large volumes observed by the radar pulse volumes later.

Throughout this study we use the well-known gamma function to represent the DSD (Ulbrich 1983) given by

$$N(D) = N_0 D^{\mu} \exp(-\Lambda D), \tag{1}$$

where D is the drop diameter, μ is the shape parameter, which increases as the breadth of the DSD decreases, and Λ is the slope parameter, which increases with the slope of the large size portion of the spectrum and also affects the DSD breadth.

Chandrasekar et al. (2003) cast some doubt on the validity of Eq. (1). They believe the downward curvature and therefore decreased numbers of small drops relative to an exponential distribution is merely an attempt to fit an experimental DSD in which the small diameter drops are underestimated by the instrument. They conclude that this is especially true for the disdrometer. However, as shown in Atlas and Ulbrich (2000), the gamma DSD is a realistic representation of the actual DSDs observed at the surface during the convective regions of thunderstorms, especially when it appears that equilibrium DSDs exist in upper levels of the storm. Because of the size sorting by the updraft aloft, the numbers of small drops can be considerably less than that predicted by an exponential DSD. Sauvageot and Lacaux (1995) also conclude that the small drop masking effect "is only of minor consequence and cannot explain the rarity of small drops in tropical rainfall."

For ease of the reader, Table 1 includes the set of equations that are used in this work. It is an extension (with corrections) of Table 10.4 in Rosenfeld and Ulbrich (2003).

Section 2 describes the environment, the drop growth processes, and the properties of the DSDs observed in Brazil during the TRMM LBA (hereinafter simply LBA or Brazil) experiment and those at Arecibo. The latter section also deals with the physical interpretation of the behavior of the parameters of the gamma distribution and how they influence the relations between radar reflectivity (Z at horizontal polarization), differential reflectivity (ZDR) and the properties of the rainfall. Section 3 focuses on the climatological variations of the raindrop size spectra in convective portions of storms in maritime and continental regimes and the responsible physical mechanisms. Section 4 treats the resulting Z–R relations and section 5 presents the summary and conclusions.

TABLE 1. Relations between sets of rainfall parameters as found from their theoretical definitions in terms of a gamma drop size distribution. All relationships involving R assume a power-law fall speed relation of the form $v(D) = 16.7D^{0.67}$ (Atlas and Ulbrich 1977), where $v(D)$ is in meters per second and D is in centimeters.

Parameters	Relation			Equation No.
Gamma DSD		$N(D) = N_0 D^{\mu} \exp(-\Lambda D)$		(T1)
D_0, μ, Λ		$D_0 = (3.67 + \mu)/\Lambda$		(T2)
D_0, D_m, μ		$D_m/D_0 = (4.0 + \mu)/(3.67 + \mu)$		(T3)
σ^2/D_m^2		$\sigma_m^2/D_m^2 = 1/(4 + \mu)$		(T4)
Z, R	$Z = AR^b$,	$A = \dfrac{10^6\Gamma(7 + \mu)N_0^{-2.33/(4.67+\mu)}}{[33.31\Gamma(4.67 + \mu)]^{(7+\mu)/(4.67+\mu)}}$	$b = \dfrac{7 + \mu}{4.67 + \mu}$	(T5)
D_0, R	$D_0 = \varepsilon R^{\delta}$,	$\varepsilon = \dfrac{3.67 + \mu}{[33.31N_0\Gamma(4.67 + \mu)]^{1/(4.67+\mu)}}$	$\delta = \dfrac{1}{4.67 + \mu}$	(T6)
N_T, R	$N_T = \xi R^{\eta}$,	$\xi = \dfrac{\Gamma(1 + \mu)N_0^{3.67/(4.67+\mu)}}{[33.31\Gamma(4.67 + \mu)]^{(1+\mu)/(4.67+\mu)}}$	$\eta = \dfrac{1 + \mu}{4.67 + \mu}$	(T7)
W, R	$W = \zeta R^{\kappa}$,	$\zeta = \dfrac{\pi\Gamma(4 + \mu)N_0^{0.67/(4.67+\mu)}}{6[33.31\Gamma(4.67 + \mu)]^{(4+\mu)/(4.67+\mu)}}$	$\kappa = \dfrac{4 + \mu}{4.67 + \mu}$	(T8)
N_W, W, D_m		$N_W = \dfrac{4^4}{\pi\rho_w}\left(\dfrac{W}{D_m^4}\right)$		(T9)
N_W, N_T, μ		$N_W = \dfrac{4^4(1 + \mu)(2 + \mu)(3 + \mu)}{6(4 + \mu)^3}\left(\dfrac{N_T}{D_m}\right)$		(T10)
$f(\mu)$		$f(\mu) = \dfrac{6}{3.67^4}\dfrac{(3.67 + \mu)^4}{\Gamma(4 + \mu)}$		(T11)

2. Observations

a. Brazil—LBA

1) THE ENVIRONMENT AND MICROPHYSICS

The storm treated here was discussed in greater detail by AW; however, they omitted the in-depth treatment of the DSDs. The storm passed over the profiler radar at the Ji Parana airport (Rondonia, Brazil) on the afternoon of 17 February 1999. The large-scale easterly wind regime was controlled by the ITCZ located to the north of the Rondonia region; however this storm had a southwest trajectory over the airport. Easterly wind regimes transport more aerosols and higher convective available potential energy air (CAPE = 2158 J Kg^{-1}) as a result of the dry continental fetch than do westerly wind regimes in which the airflow is over the moist aerosol-poor environment of the Amazon basin (Halverson et al. 2002). The storm was intense; it reached a height of 14 km and the maximum updraft exceeded 24 m s^{-1}. However, most of the precipitation development occurred by warm processes (AW). AW concentrated on the anatomy of the storm as observed by the array of instruments; here we focus on the characteristics of the drop size spectra.

Figure 1 shows the time record of the rain rate R (dBR), radar reflectivity factor Z (dBZ), the median volume diameter D_0 (mm), and the parameter N_W (dBN) throughout the 27 min of the storm {N_W (dBN) = $10 \times \log_{10}[N_W(\mathrm{m}^{-3}\ \mathrm{cm}^{-1})]$}. Here, N_W is the normalizing constant defined as the intercept of an equivalent exponential DSD with the same water content W (Testud et al. 2001; BC). See Table 1 for the relation of N_W to the conventional total drop number concentration N_T, and the parameters mean volume diameter D_m, liquid water content W, and the shape μ. Except for the first two and last three minutes, the entire period is marked by very large D_0 (2–3 mm), large Z (45–53 dBZ), and large R ($R_{\max} \sim 120$ mm h^{-1}).

The method of calculating the DSD parameters is described by Zhang et al. (2003). They used the second, fourth, and sixth moments of the distribution. This method tends to place emphasis on the middle of the drop size distribution and thus avoids any difficulties associated with undercounting of small and large drops. Nevertheless, as mentioned earlier, the decreasing

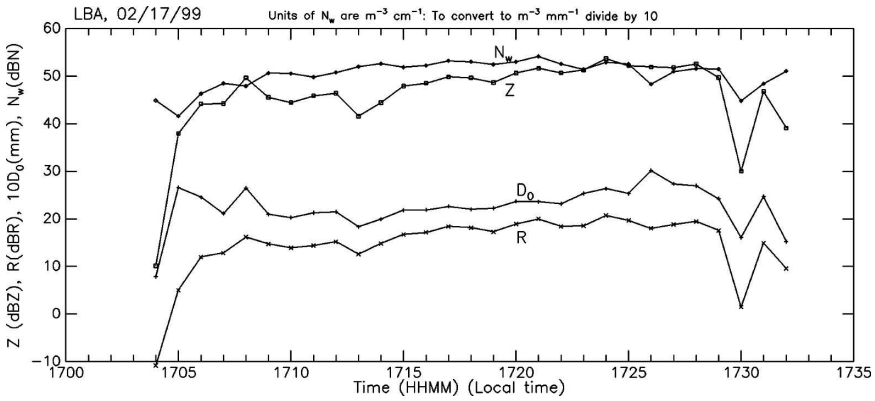

FIG. 1. Time dependence of R (dBR), Z (dBZ), D_0 (mm), and N_W (dBN) at Ji Parana, Amazonia, Brazil, during the LBA experiment on 17 Feb 1999, in local time. Note ordinate scales for each parameter $\{N_W(\text{dB}N) = 10 \times \log_{10}[N_W\ (\text{m}^{-3}\ \text{cm}^{-1})]\}$.

numbers of small drops is considered to be real for the tropical storms and cannot be explained entirely by instrumental effects.

As indicated above, the entire period of rain is convectively generated as shown by simultaneous observations made with the vertically pointing 915-MHZ radar profiler (AW, their Fig. 1). Reflectivity exceeded 43 dBZ, and the mean upward Doppler velocity exceeded 8 m s^{-1} from near the surface up to the 0°C level throughout most of this period.

AW showed that the dominant particle growth occurs almost entirely below the 0°C level during the initial phase (i.e., leading edge) of the storm between 1700 and 1715 local time (LT). The major growth takes place where the drops are approximately balanced by the updraft. The near balance of the drops extends the residence time for operation of the collision, coalescence, and breakup (CCB) process so that the DSD reaches equilibrium. It is evident from the profiler observations for 1410 LT (not shown) that all the growth is occurring below the 0°C level.

The draft also partitions the DSD into small particles that rise and fall out elsewhere if they survive, and large ones that reach the surface in narrow distributions. From the base of the updraft to the surface the fall speed of the large drops is nearly constant and corresponds approximately to the updraft speed. This is particularly relevant because it suggests that the largest drops and the associated radar reflectivity are controlled by the updraft so that the appropriate Z–R relation may be estimated from the storm intensity.

In the later stage of the storm, following 1715 LT, the updraft rises above the 0°C level and increases in speed so that one finds ice particles balanced in the 6.5- to 8-km layer, and the largest particles have fall speeds of ≈9 to 18 m s^{-1} corresponding to maximum hail size of about 1.5- to 2-cm diameter. This condition is associated with the onset of a sharp increase in lightning. Although the melting particles contribute to the rain during this period, the 0°C level is sufficiently high (5 km) that the CCB dominates the nature of the DSD at the surface. This is supported by the continued nearly constant values of Z and D_0 between 1705 and 1730 LT. The reader is referred to Hu and Srivastava (1995), Atlas and Ulbrich (2000), AU1, and AW for further discussion of the mechanisms responsible for the growth of the large drops and near-equilibrium DSDs and for other references.

2) PROPERTIES OF THE DROP SIZE DISTRIBUTIONS

Figure 2 shows the μ–Λ–D_0 plot following the method used in AU1. For simplicity we shall refer to this as the gamma parameter diagram (GPD). The lines of constant D_0 depict the relation $D_0 = (3.67 + \mu)/\Lambda$ in Table 1. As indicated in Fig. 1, all but one point fall in the range $2.0 < D_0 < 3.0$ mm. The shape parameter μ ranges from $\mu \approx 3$ to 11.5 while the slope parameter Λ ranges only from 2 to 7 mm^{-1}, respectively. The value of $\mu = 11.5$ corresponds closely to the very narrow DSD reported by Atlas and Ulbrich (2000, their Fig. 2c). The D_0 and μ values are the largest found in any of the four storms considered here and in AU1.

Figure 3 is a plot of ZDR versus Z for this storm. Because of the uniformly large D_0s on the right-hand ordinate, ZDR ranges from about 0.9 to 2 dB for $40 < Z < 53$ dBZ and falls along the relation ZDR = $0.093Z^{0.28}$, almost identical to that for the Arecibo storm (as shown later in Fig. 6). The differential reflectivity values are based upon the ZDR–D_0 relation of BC (section 7.1) shown in the legend.

The ZDR–D_0 relation depends upon μ, D_0, and the

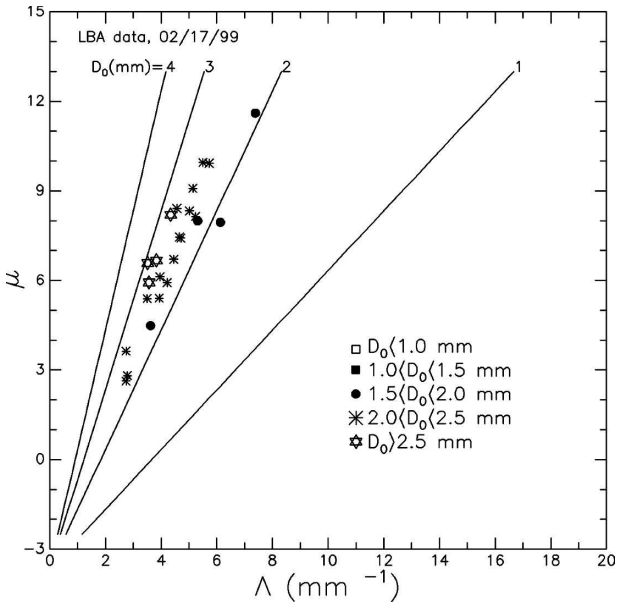

FIG. 2. Plot of μ vs Λ with isopleths of D_0 on the GPD for LBA on 17 Feb 1999. The entire period is classified as convective. Symbols correspond to drop diameters indicated in legend. Note that all but one sample falls in the range of 2–3 mm. All samples are of 1-min duration.

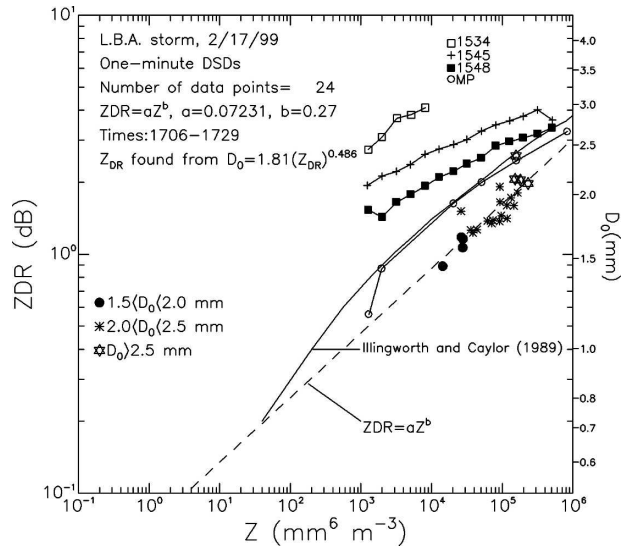

FIG. 3. Plot of ZDR (dB) vs Z (mm^6 m^{-3}) for LBA data as in Figs. 1 and 2. The scale of D_0 on the right ordinate is based upon the ZDR–D_0 relation in the legend along with the ZDR–Z regression relation. The points with the legend in the top right correspond to the time sequence of observations made with the NCAR CP-2 radar in Alabama (Fig. 7.27 of Bringi and Chandrasekar 2001). The solid curve is that of Illingworth and Caylor (1989). See text for details.

maximum diameters in the DSD. The larger the drops, the greater the polarization shape effect. BC have developed a mean fit assuming $-1 < \mu \leq 5$, $0.5 \leq D_0 \leq 2.5$ mm, and the DSD intercept N_0 chosen to be consistent with thunderstorm rainfall rates. Clearly, the narrower the DSD (i.e., larger μ), the larger the number of drops in the larger sizes, the greater the drop shape effect, and the larger the ZDR. This is very likely the reason for the somewhat larger values of ZDR shown by Bringi et al. (2002, their Fig. 2) and the very large ZDR values reported by Zhang et al. (2006, their Fig. 4) for the leading edge of convective rain. Similar behavior of the ZDR values will be seen later (in Fig. 6) for Arecibo, where the data are constrained within a narrower range of large Z and corresponding large drop sizes of $2.0 < D_0 < 3.0$ mm. We shall discuss this further in section 2b(3). In view of the large scatter in the ZDR–D_0–Z relations found by BC (their Figs. 7.20 and 7.23) and by Zhang et al. (2006, their Fig. 4) we shall continue to use the ZDR–D_0 relation shown in Fig. 3 while recognizing its limitations for the large μ and D_0 values.

b. Puerto Rico—Arecibo

1) THE ENVIRONMENT

The next set of drop size distribution observations was acquired at the National Astronomy and Ionosphere Center (NAIC) in Arecibo during October 1998. The data were collected as a part of an experiment in which the NAIC dual-wavelength (UHF and VHF) Doppler radars, a UHF interferometer, an electric field mill, and surface meteorological instrumentation were used to observe tropical thunderstorms. The goal of the experiment was to determine the transport of NO_x formed in lightning flashes into the stratosphere by circulation patterns in and around thunderstorms. Preliminary results from the experiment were described in Ulbrich et al. (1999).

Drop size distributions observed by the JWD were collected at NAIC on 20 days during September and October 1998. The instrument dead time correction was applied to calculations performed in this work, and it was found to have only a minor effect on integral parameters calculated from the DSDs.

Only seven days on which data were collected involved storms with total precipitation depth exceeding 10 mm. The strongest of the storms occurred on 15 October and involved a total depth of rainfall of 47.2 mm and displayed a structure similar to that which has been observed for tropical storms in Tropical Ocean and Global Atmosphere Coupled Ocean–Atmosphere Response Experiment (TOGA COARE; hereinafter TOGA) as described by Atlas et al. (1999). The storm

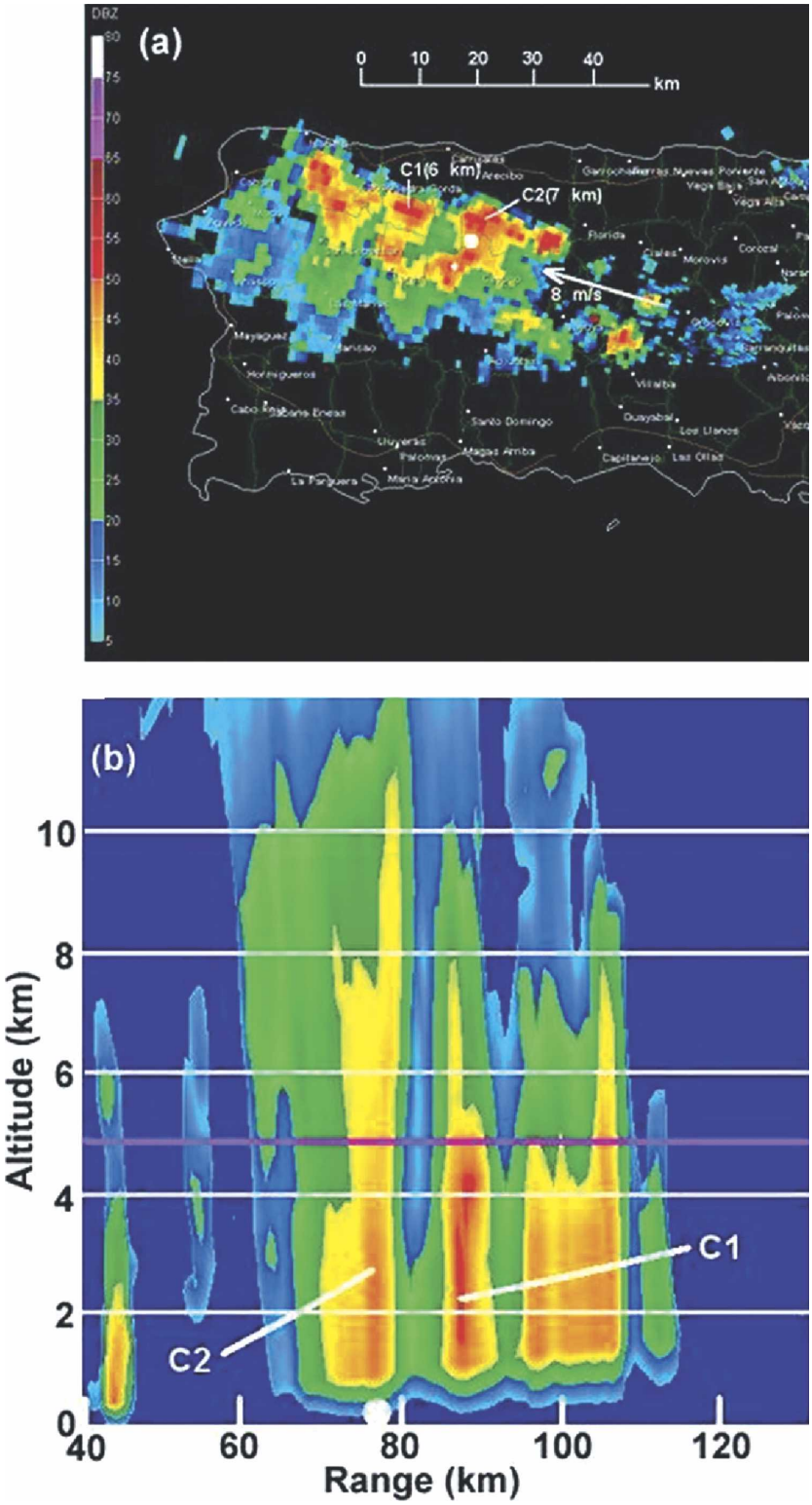
(a)
DBZ
0 10 20 30 40
km
C1(6 km)
C2(7 km)
8 m/s
(b)
Altitude (km)
Range (km)
C1
C2

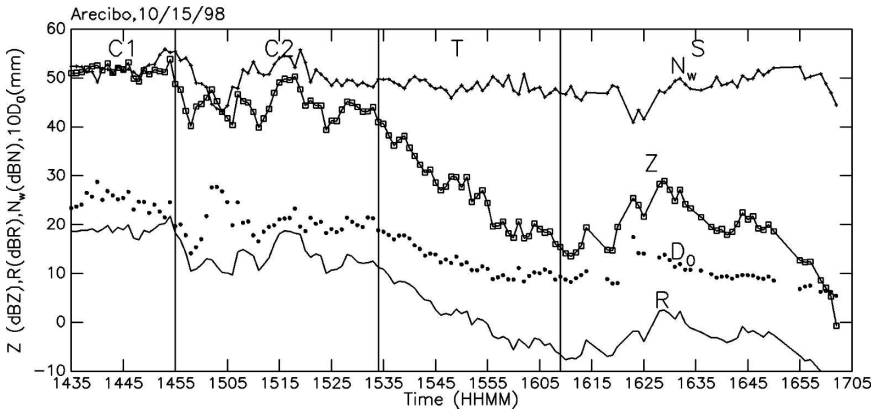

FIG. 5. Time dependence of R (dBR), Z (dBZ), D_0 (mm), and N_W (dBN) at Arecibo, Puerto Rico, on 15 Oct 1998 in local time. Note ordinate scales for each parameter. The record has been divided into the large-drop, large-Z region of convective segments (C1, C2), the progressively decreasing Z in the transition (T) region, and the remaining stratiform (S) rains {N_W (dBN) = $10 \times \log_{10}[N_W\ (\mathrm{m}^{-3}\ \mathrm{cm}^{-1})]$}.

had fairly well defined periods that could be classified as C, T, and S as shown in Fig. 4. The rules for the latter classification are as follows: 1) the C region is marked by Z > ≈45 dBZ and $D_0 > 1.5$ mm, 2) the S region is marked by considerably smaller values of Z and D_0, and 3) the T rain was identified as that between C and S. When the radar profiler or scanning radars were available we also used the structure of the reflectivity and Doppler velocity patterns.

On 15 October, convection was initiated on the windward (eastern) slopes of the interior mountains of Puerto Rico at about 1315 LT with individual cells propagating toward the west-northwest. By 1430 LT the cells had grown to maturity as they passed over the location of the disdrometer, attaining maximum altitudes of approximately 14 km, equal to those observed in the LBA storm. The lowest-level (0.4°) plan position indicator (PPI) at 1456 LT is shown in Fig. 4a along with the Range Height Indicator (RHI) at 289° azimuth, which passes over the JW disdrometer (Fig. 4b). The white dots on both the PPI and RHI correspond to the position of the JWD. The PPI and RHI are discussed further below.

A sounding of meteorological parameters for San Juan, Puerto Rico, at 1600 LT (not shown) showed the lower-level environmental winds out of the east-southeast at about 10–15 kt (1 kt ≈ 0.5 m s^{-1}); individual cells in the storm moved at 15 kt in the same direction. Environmental winds backed into the north at about 10 km and eventually at higher levels to the west-northwest at about 15 km. This is reflected in the structure of the upper-level clouds associated with the storm that turn to the south in the middle levels and eventually toward the east in the highest levels. The CAPE = 3348 J Kg^{-1}, thus indicating a very unstable atmosphere. The surface dry bulb and wet bulb temperatures were 28° and 24°C, and the 0°C level is at 4.8 km, also close to that in Brazil. As noted in the Brazil case, the constancy of Z and D_0 during the first 20 min of the record (Fig. 5) suggests that the CCB process is effectively in control despite the likelihood of melting hail from above. Since the thunderstorm cells on this date were formed on the windward slopes of the interior Puerto Rican mountains and not over the ocean, it has been concluded in this work that the storm was of continental character.

←

FIG. 4. (a) PPI display of reflectivity factor for the Arecibo storm at 1456 LT. The colors corresponding to the Z(dBZ) are shown on the scale to the left. The red areas correspond to Z levels of 50–55 dBZ. The scale shown at the top of the display indicates the distance scale. The white arrow shows the direction of movement of the cells to the west-northwest at 8 m s^{-1} (≈16 kt). The solid white dot indicates the location of the disdrometer. The labels C1 and C2 indicate cells associated with the C1 and C2 convective regions referred to in the text. The numbers associated with these labels are the altitudes of the 50-dBZ contours. (b) RHI display of reflectivity factor for the Arecibo storm along the 289° azimuth for the time 1517 LT. The solid white dot at the bottom of the diagram is the location of the disdrometer. The horizontal purple line is the 0°C level. The horizontal white lines are lines of constant altitude above sea level and are labeled with their height in kilometers. The horizontal axis is labeled with the distance from the San Juan National Weather Service radar (km). The color scheme for the reflectivity-factor levels is the same as that used in (a).

2) Properties of the drop size distributions

Figure 5 presents the time plot of Z, R, D_0, and the generalized total number concentration N_W. The rain lasted for a period of 2.5 h, longer than any other of the storms treated here or in AU1. It began with a 20-min convective (C1) burst of large drops with $Z \approx 50$–53 dBZ, $R \approx 100$ mm h^{-1}, and $D_0 \approx 2.5$–3 mm. This was followed by a 38-min period with fluctuating values of all the parameters. However, Z exceeds 45 dBZ and $D_0 > 2$ mm for most of this period; thus, it corresponds to a convective period, which we have labeled C2. This is consistent with the existence of an adjacent convective cell such as occurs in a multicell storm (Chisholm 1973). Cells C1 and C2 at 1517 LT are shown in the PPI and RHI of Fig. 4. We have compared the sequence of Z values over the JWD on 22 successive low-level PPIs between 1425 and 1615 LT (not shown) and found them to be in very good agreement with those computed from the drop size spectra. The period 1534 to 1610 LT, during which Z and D_0 fall precipitously, is the transition period, and the remainder of the record corresponds to the stratiform rain. (The associated Z–R relations and cumulative contributions of each zone to the total rainfall are presented in Table 3, to be discussed later.)

Note that $N_W \approx 10^5$ m^{-3} cm^{-1} during the C1 period, oscillates around that value during C2 and falls slightly lower during the lengthy T and S rains. This N_w is associated with $N_T \approx 500$–1000 drops m^{-3} during the C1 and C2 periods. The sharp changes in N_w and D_0 during C2 are consistent with those in Z and R for an equivalent exponential DSD. Moreover, although D_0 varies between 2 and 3 mm, the DSDs during this period are reasonably close to equilibrium.

Figure 6 shows the Gamma Parameter Diagram where rain types are colored red (C1), purple (C2), green (T), and blue (S). Except for one sample, the C1 period is marked by $2.5 < D_0 < 2.9$ mm, very close to those in the Brazil storm. It is likely that the 1-min samples reflect the actual physical variations and are not due to sampling errors. During the stratiform (S) period the D_0 values range from about 0.5 to 1.6 mm and are reasonably consistent with the regression curve reported by Brandes et al. (2003) and shown in Fig. 6 that we have previously suggested is due to the stratiform and transition rains with $0.5 < D_0 < 1.5$ mm in their Oklahoma storms (AU1).

3) Differential reflectivity versus reflectivity

Figure 7 displays the relation between the differential reflectivity ZDR versus Z in colors corresponding to those in Fig. 6. With few exceptions log(D_0) and log(ZDR) increase linearly with log(Z) from S to T to C rains as expected from Fig. 6. This contrasts with the TOGA behavior where the T rains showed the smallest D_0 and ZDR values. The relation is ZDR = $0.109Z^{0.27}$. The large scatter in ZDR during C2 reflects that in D_0 shown in Fig. 6. The purple curve corresponds to the relation determined by Illingworth and Caylor (1989, hereinafter IC) and is based on theoretical calculations of ZDR and Z using a gamma DSD with $\mu = 0$ and a maximum diameter $D_{\max} = 8$ mm. The IC paper also shows actual measurements of ZDR and Z made with the giant Chilbolton (England) 10-cm radar. That radar, with a 0.25° beam, used a typical sample volume of 300 m^3 so that it is expected that it would have included a few of the largest drops up to 8- or even 10-mm diameter. Also, IC indicate the accuracy of the ZDR measurements to be ±0.1 dB, and they show average incremental values of Z and ZDR as determined by the Chilbolton radar spanning an approximate range of $30 < Z < 60$ dBZ. Those data are not shown in Fig. 7; however, their theoretical purple curve shown in Fig. 7 is in excellent agreement with their experimental data. In IC, it is suggested that the agreement of this curve with that expected for an exponential DSD with $\mu = 0$

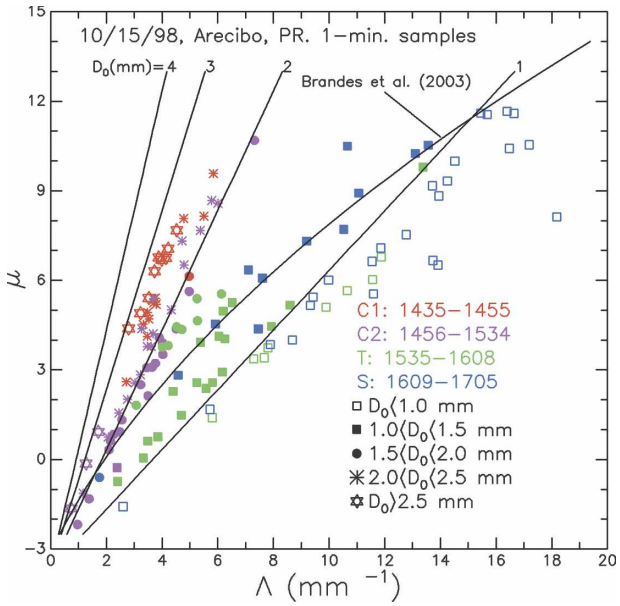

FIG. 6. Plot of μ vs Λ and D_0 on the GPD at Arecibo on 15 Oct 1988. The color code corresponds to the C, T, and S regions of Fig. 5. The symbols correspond to the drop sizes shown in the legend. All samples are of 1-min duration. Note that the convective D_0 samples (C1: red, C2: purple) are mostly close to 3 and 2 mm, respectively. The one sample at 4.1 mm has been omitted (see text). The smooth black curve corresponds to the regression relation of Brandes et al. (2003) and falls between about 0.5 and 1.5 mm in the region of stratiform rain.

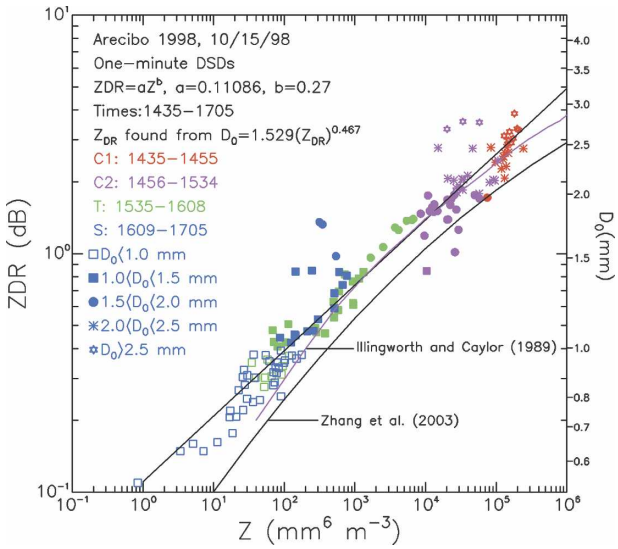

FIG. 7. The ZDR–Z–D_0 scattergram for Arecibo data of Fig. 6. The color code is the same as in Fig. 6 and the symbols correspond to the drop size ranges shown in the legend. Note the ZDR–Z regression relation in legend and close correspondence to the purple curve based upon theory and radar observations of Illingworth and Caylor (1989). The black curve is that of Zhang et al. (2003).

and D_{max} = 8 mm indicates the probable existence of such large drops in the huge radar pulse volumes. One notes remarkable agreement between the IC averaged data and the present Arecibo regression relation based upon surface-measured drop size data in a single storm. The same is true for the Brazil observations in Fig. 3. This could be a coincidence. Nevertheless, it is suggestive that the small-sample surface drop size measurements are reasonably representative of what is measured by a radar of high resolution. The one caveat follows.

On the other hand, one must raise the question as to whether or not the narrow DSDs observed by the JWD are due to truncation of the small numbers of both large and small drop sizes resulting from the small samples by the JWD. There was one sample with D_0 = 4.1 mm, which may be an indication of such an effect. However, it was the very first sample and is due to the very small number of giant drops at the leading edge of the storm. We believe that it is unrepresentative of the subsequent samples and have omitted it from the time record in Fig. 5. Otherwise, the variability of the D_0 points within the 20 min of the C1 period is so small as to indicate that the sample size is adequate. Thus, we suggest that the near-equilibrium large D_0 values in Figs. 1 and 5 imply that they are representative of the large radar volumes aloft. Although the breadth of the DSDs is probably reduced by the small sample sizes, it is difficult to imagine that the small JWD sample sizes would have resulted in as narrow a DSD as μ = 6–12. We therefore believe that the spectrum breadths in the C periods of Brazil and Arecibo are only slightly broader aloft than indicated by the range $3 < \mu < 12$ observed by the JWD at the surface. Again, one must recall the common experience of monodisperse large drops that occur in the early stages of convective storms everywhere.

With regard to the prior discussion, we refer to Fig. 7.27 of BC that shows the evolution of the ZDR–Z during an intense storm observed by the 10-cm wavelength, 1° beam of the National Center for Atmospheric Research (NCAR) CP-2 radar in Alabama. We have overlaid their data on Fig. 3. One sees that the observations begin at 1534 (open squares) with a period of moderate $Z < 40$ dBZ, but large drops ($\approx 2.4 < D_0 < 3.0$ mm) and large ZDR. The Z values are small because of the small number of drops. Eleven minutes later at 1545 (plus signs) Z_{max} reaches 55 dBZ and $2.0 <$ ZDR < 4.0 dB (i.e., $\approx 2.0 < D_0 < 3.0$ mm). This corresponds to what we have identified as the C1 and C2 periods with near-equilibrium DSDs in the present work. Three minutes later at 1548 (filled squares) ZDR decreases to $1.4 <$ ZDR < 3.4 dB (i.e., $\approx 1.7 < D_0 < 2.7$ mm), the transition period, and finally at 1555 (open circles) to the values corresponding to the Marshall–Palmer (1948) relation for stratiform rain. Such behavior is consistent with our division of the rain into periods of C, T, and S segments. If plotted on the ZDR–Z graph of Fig. 7, the Alabama data mimic the behavior of the Arecibo storm with the exception of the initial observations of 1534. However, the 1534 Alabama data correspond closely to the 1704–1705 LT initial observations of reduced D_0 and Z in the LBA storm (Fig. 1).

It is also interesting to compare the vertical cross sections of Z and ZDR observed in what is described as a "tropical" storm that produced a flash flood in Fort Collins, Colorado (as shown in BC's Fig. 7.29), with that shown in Fig. 5 of AW during LBA. There is no evidence of a bright band; the large Z (up to 50 + dBZ) and the $1.0 <$ ZDR < 3.0 dB occur entirely below the 0°C level. This is virtually a mirror image of AW's Fig. 5 both geometrically and in terms of Z and ZDR. However, BC attribute the large ZDRs to the melting of graupel and hail, while AW found that the drop growth was dominated by collision, coalescence, and breakup in the updraft below the 0°C level until later in the storm when the strong updraft extended above that level. We now note that it is probably the high (4.8 km) 0°C level that facilitates the effectiveness of the CCB process during the entire period of convective rains.

In Fig. 7 we note that the initial convective (C1) pe-

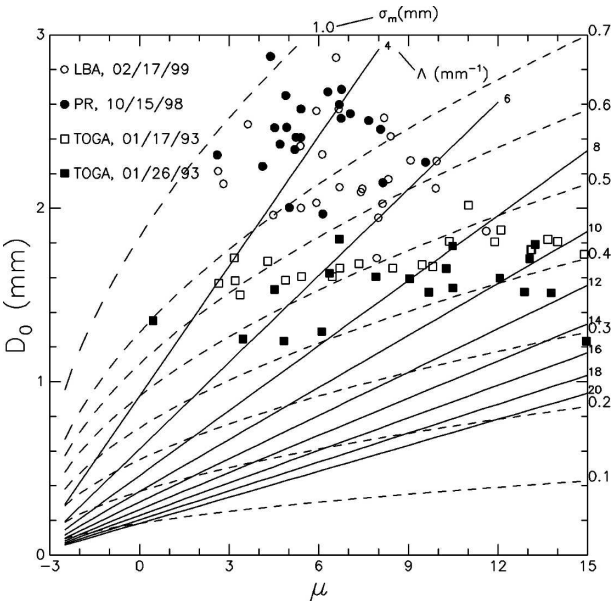

FIG. 8. A plot of D_0 vs μ for convective samples from two days of TOGA COARE, Arecibo, and LBA as shown according to the symbols in the legend. The maritime TOGA points fall between about $D_0 = 1.4$ and 2.0 mm and $\mu = 3$ and 15. The nearly constant D_0 values indicate equilibrium DSDs. The continental LBA and Arecibo D_0 samples fall almost entirely within 2 and 3 mm, while μ ranges between 3 and 10. The modest range of D_0 indicates near-equilibrium DSDs. The dashed curves are isopleths of normalized std dev of the mass spectrum $\sigma_m = \sigma_M/D_m$.

riod is marked by a sharp limit at $Z = 53$ dBZ, $1.5 < D_0 < 3$ mm, and $2 <$ ZDR < 4 dB. Such an asymptotic bound is close to those found by a variety of investigators (BC; Bringi et al. 2002; Sauvageot and Lacaux 1995; Rosenfeld and Ulbrich 2003; Uijlenhoet et al. 2003). However, it is worth noting that IC, using the giant Chilbolton radar, report values of $4 <$ ZDR < 6 dB at $54 < Z < 60$ dBZ. One must wonder whether the difference in these large values from those reported by poorer-resolution radars is due to the sample size.

3. Climatological behavior: Continental versus maritime

Here we examine the convective (C) periods in the continental Tropics as compared with those previously found in the maritime Tropics in AU1. This subject has also been discussed in another fashion by BRAL. Figure 8 presents the data on a more general GPD in which we have added isopleths of the normalized mass spectrum width $\sigma_m = \sigma_M/D_m$. The symbols correspond to TOGA on 26 January 1993 (filled squares) and 17 February 1993 (open squares), LBA (open circles), and Puerto Rico (filled circles). The narrow ranges of D_0 in all cases indicate equilibrium-type DSDs; the LBA values are somewhat broader than the others. We have omitted the C2 convective period from Arecibo because the D_0 values there are similar to those in C1. The maritime D_0 values are clearly smaller than the continental ones, with both μ and Λ extending over a broader range. This is again due to the fact that $D_0 = (3.67 + \mu)/\Lambda$ so that for constant D_0 μ must increase with Λ; the less so, the larger D_0 is. This is physically consistent with the fact that the slope of the tail of a gamma DSD increases as the distribution narrows. The increase in D_0 from about 1.5 to 1.7 mm for the maritime TOGA samples to values of 2.0–2.6 in LBA and a bit more at Arecibo is also in line with the increase in the vigor of the storms as indicated by the soundings and the updraft strength. This was found by Atlas and Ulbrich (2000) based upon surface and airborne measurements of DSD and updraft strength during TOGA and by AW using a radar profiler to estimate the updrafts and surface observations of DSD in LBA. Note also that at constant D_0 the mass spectrum width σ_m decreases with increasing μ, as mentioned earlier on intuitive grounds. Such behavior is also indicated by Eq. (T4) in Table 1.

We have previously discussed the CCB process involved in generating equilibrium DSDs in which D_0 increases with updraft strength. It has also been described in greater depth by AU1 and AW. The CCB mechanism was shown to dominate in the early stages of the LBA storm. It is only later in the storm's life and further back from its leading edge where the updraft extends to heights above the 0°C level that graupel and hail produce melt water to add to the warm rain produced below. This is also the period during which lightning begins or increases in intensity (AW). These are the reasons that we find equilibrium or near-equilibrium DSDs in the initial convective rains and why the median volume drop sizes are larger in the tropical continental storms. BRAL also state that "at high rain rates, the radar and disdrometer D_0 values range toward a stable value around 1.7–2.0 mm, reflecting the tendency to equilibrium-like distributions where drop breakup and coalescence are in near balance." We qualify this statement to note that the rain rates often vary during the equilibrium period (AU1) as a result of the changes in number concentration.

BRAL have also shown interesting features of the properties of stratiform and convective storms in a variety of climatic regimes. Here we would like to clarify and extend their findings. They also use the mass weighted diameter D_m in that work. The relation of D_m to D_0 is shown in Eq. (T3) of Table 1. First of all their Fig. 5 shows that the spread σ_m/D_m of the mass distribution decreases with μ in a manner similar to that

expected from the gamma distribution as indicated by Eq. (T3) in Table 1. This is also indicated in our Fig. 8. For the eight regions treated in BRAL (i.e., Papua, New Guinea, to Darwin, Australia, to Austria, and Colorado, etc.) they conclude that "the average shape of the DSD can be represented by the gamma form . . . with $\langle\mu\rangle$ ranging from 1 to around 10." The most tropical, near-oceanic regime is Papua with $\langle\mu\rangle = 9$. This is very similar to the average value found in TOGA (AU1). BRAL also reported an outlier of $\langle\mu\rangle \approx 1$ (very close to that for the Marshall–Palmer DSD) for a convective storm in Colorado.

BRAL then display a plot of $\log\langle N_W\rangle$ versus $\langle D_m\rangle$, where N_W is defined by $N_W = (256/\pi\rho_w)(W/D_m^4)$ and $\rho_w = 1.0$ gm cm^{-3} is the density of water (Table 1). The DSD may then be expressed as $N(D) = N_W f(\mu)(D/D_0)^\mu \exp[-(3.67 + \mu)D/D_0]$ [where $f(\mu)$ is given by Eq. (T11) in Table 1]. Thus the more water is concentrated in large D_m, the smaller N_W is (BRAL, their Fig. 11) and the narrower the DSD is (i.e., μ is larger; BRAL, their Fig. 5).

BRAL then show that on a plot of N_W versus D_m their data divide into two distinct clusters corresponding to maritime and continental convective storms. For maritime storms, $\log_{10}[\langle N_w\rangle$ (m^{-3} mm^{-1})$] \approx$ 4–4.5 with $\langle D_m\rangle \approx$ 1.5–1.75 mm, that is, a large concentration of medium-sized drops. The second "cluster" is characterized by $\langle D_m\rangle \approx$ 2–2.75 mm and average $\log_{10}[\langle N_w\rangle$ (m^{-3} mm^{-1})$] \approx$ 3–3.5 and corresponds to the regime varying from the U.S. high plains (Colorado) to continental (Graz, Austria) to subtropics (Sydney, Australia) to Tropics (Arecibo). This "continental like" cluster may be defined as that which reflects a DSD characterized by a smaller concentration of larger-sized drops as compared with the maritime-like cluster.

To compare our data with those of BRAL, Fig. 9 shows only observations from the *convective* (C) segments of the two maritime and two continental storms on an N_W–D_m plot coded as indicated in the legend. For clarity we have also superimposed curves of rainwater content W and isopleths of $\mu = 3$ and 9 for each of the sets of values of $10\log_{10}(N_T) = 20$, 25, and 30 dBN_T, where N_T (m^{-3}) is the total number concentration. Superimposed upon the scatterplot are two ellipses that contain most of the maritime and continental data for "convective" storms in Fig. 11 of BRAL. We must recall that their values for convective storms cover the entire storm, however, including what we have identified as the convective, transition, and stratiform sections.

We see that there is good agreement between the bulk of the 1-min samples in the two TOGA storms with the BRAL maritime ellipse and between the LBA

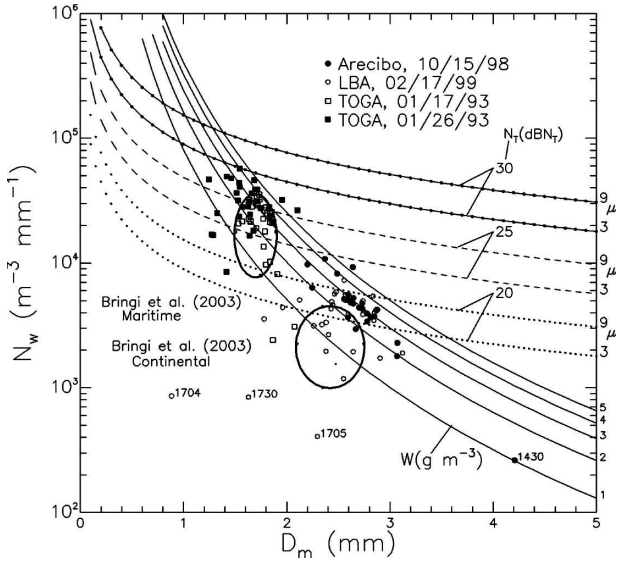

FIG. 9. A plot of the generalized number concentration N_W (m^{-3} mm^{-1}) vs the mass weighted mean diameter D_m (mm) with contours of water content W (g m^{-3}) and contours of $\mu = 3$ and 9 for total number concentrations N_T (dBN_T) of 20, 25, and 30. The open circles correspond to the continental convective samples only in LBA; the solid circles are for Arecibo. The open and solid squares correspond to the maritime convective points observed during TOGA COARE on the days indicated in the legend. The ellipses correspond to the maritime and continental clusters reported by Bringi et al. (2003) and agree remarkably well with the individual one-min sample of convective rain in both regions. The points labeled with times 1704, 1705, 1730, and 1430 occur either at the very beginning or the end of the convective period and are considered to be unrepresentative $\{N_T\,(\mathrm{dB}N_T) = 10\log_{10}[N_T\,(\mathrm{m}^{-3}\,\mathrm{cm}^{-1})]\}$.

(open circles) and Arecibo (filled circles) convective segments with their continental ellipse. (We have omitted the data corresponding to convective period C2.) It is also significant that both ellipses are centered below the center of the bulk of the corresponding data for our *convective* storm segments. This is due to the inclusion of transition and stratiform data within each of the BRAL convective storms. Their Fig. 10 shows how the average N_W decreases with D_m in stratiform storms from about 10^4 m^{-3} mm^{-1} at $D_m = 1.25$ mm to 10^3 m^{-3} mm^{-1} at $D_m = 1.75$ mm, thus accounting for the lower centers of the ellipses for the BRAL data. The latter behavior may also be discerned from the (N_w, W, and D_m) relation [Eq. (T9) in Table 1]. For constant rainwater content W, N_W decreases as $(D_m)^{-4}$, so that the increase in D_m from about 1.5 to 2.5 mm corresponds to about an eightfold decrease in N_W.

One also notes the three very low N_W points for LBA and the one low point for Arecibo at $D_m = 4.1$ mm. Three of these occurred mainly at the very start, as expected from long experience with the few large drops

TABLE 2. The physical properties of the convective portions of maritime and continental convective storms with equilibrium or near-equilibrium DSDs.

Property	Maritime	Continental
D_0 (mm)	1.3–1.7	2.0–3.0
μ	3–15	3–9
Λ (mm^{-1})	4–12	3–6
W (g m^{-3})	1–4	0.5–2.0
N_W (m^{-3} mm^{-1})*	2×10^4	2×10^3
Process	CCB—warm	CCB—mostly warm
Colorado**		Melt graupel–hail

* From BRAL.
** This is an outlier.

observed at the start of a storm. Note as well that the rainwater contents W for the convective segments of both maritime and continental storms are about the same ($\approx$1–5 g m^{-3}) and are larger than those for the storms that compose the two ellipses for the same reasons mentioned above. Moreover, we see that the maritime storms, which were previously found to have smaller D_0 and a larger range of μ (from 3 to 15 in Fig. 8), have concentrations $\approx$25–30 dBN_T, while the continental storms with $3 < \mu < 9$ have concentrations of about 20–25 dBN_T. Based upon the present observations in continental storms, those of AU1 in maritime storms, and those of BRAL in both, their typical features are summarized in Table 2.

4. Implications for remote sensing

Because the DSDs differ for maritime and continental storms, and also vary with the nature (C, T, or S) within each storm, it is evident that there will be a matrix of relations between radar reflectivity, Z, and rainfall rate, R, that is, relationships matched to the matrix of physical conditions. Table 3 presents a set of Z–R relations for the C, T, and S relations corresponding to the tropical maritime observations in TOGA as reported in Atlas et al. (1999) and AU1, and the continental observations presented here. We emphasize that the present relations differ from those expected

TABLE 3. The Z–R analyses for all storms considered in this work. Here C, T, and S label the period of rainfall as convective, transition, or stratiform. Parameters A and b are the coefficient and exponent in an empirical relation of the form $Z = AR^b$, N is the total number of drop size spectra used in the fits, and H is total depth of rainfall during each period. Times are local.

Date	Period	Times	A	b	N	H (mm)	% of total
			Arecibo, 15 Oct 1998				
	C1	1435–1455	2754	0.90	21	28.48	60.40
	C2	1456–1534	1471	0.96	39	16.83	35.70
	C1 + C2	1435–1534	906	1.13	60	45.31	96.1
	T	1535–1608	310	1.46	34	1.36	2.88
	S	1609–1705	280	1.46	54	0.48	1.02
	All	1435–1705	294	1.44	148	47.15	100.0
			LBA, 17 Feb 1999				
	C	1705–1732	817	1.16	28	23.1	100
	C$^+$	1706–1732	596	1.24	27	23.1	100
			TOGA COARE storms, 1993				
17 Jan 1993	C	1406–1431	564	1.10	26	14.22	65.35
	T	1432–1455	103	1.58	24	3.52	16.18
	S1	1456–1515	88.7	1.90	20	1.65	7.58
	S2	1516–1540	261	1.52	25	2.37	10.89
	All	1406–1540	212	1.39	95	21.76	100
26 Jan 1993	C	1158–1229	334	1.19	32	16.27	37.73
	T	1230–1359	142	1.35	90	15.49	35.92
	S1	1400–1530	289	1.41	91	6.28	14.56
	S2	1531–1640	874	1.07	70	5.08	11.79
	All	1158–1640	544	0.98	283	43.12	100
10 Dec 1992	C	0758–0820	766	1.14	27	19.05	75.85
	T	0821–0905	187	1.45	45	4.99	19.85
	S	0906–1000	223	1.13	54	1.080	4.30
	All	0754–1000	247	1.37	126	25.12	100
19 Dec 1992	C	0730–0824	99.2	1.47	55	23.63	56.50
	T	0825–1019	202	1.25	103	14.07	33.65
	S	1020–1130	252	1.61	71	4.12	9.85
	All	0730–1130	314	1.12	229	41.82	100

from the data of BRAL because they did not separate the initial convective from the transition rains.

At both Arecibo and Brazil one finds that the C rain has very large A coefficients and b exponents close to unity. The large A values are consistent with the very large values of D_0 shown in Fig. 7 and 8, and the bs accord with equilibrium-type DSDs. The A coefficient for C2 rain at Arecibo is also very large relative to those with which we are familiar (Fujiwara 1965; Battan 1973; Rosenfeld and Ulbrich 2003). None of Battan's 63 values of b and only one of those of Rosenfeld and Ulbrich is less than 1.2. But the latter corresponds to an extremely light rain rate. By comparison, the A values for the maritime convective rain segments in TOGA are considerably smaller than those for the continental convective sections because of the generally smaller values of D_0.

With the exception of 12 December 1992, all the b values for C rain are within the range $1.08 < b < 1.19$ corresponding to equilibrium-type DSDs (Atlas et al. 1999; AU1). The anomalous TOGA stratiform rain S2 of 26 January 1993 in Table 3 with large A and small b has been attributed to the melting of large snowflakes below a strong bright band and truncation of the DSD (AU1).

Of the results in Table 3, the percentage contribution of the convective portions of an individual storm to the total rainfall is of particular interest. For most of the storms it is apparent that the majority of the total rainfall is contributed by the convective elements. The results for the TOGA storm on 26 January 1993 appear not to fit this generalization well, but this has been addressed earlier. In the case of the C1 and C2 periods of the Arecibo data, we have also included the Z–R relation for the combination of the two convective regions. While the Z–R relation changes the cumulative rainfall remains the same as if measured separately. From these results, it may be concluded that it is important that the correct Z–R relation be used to measure rainfall for the convective portion since it often contributes the majority of the rainfall for the storm.

5. Summary and conclusions

This work has focused on raindrop size distributions in tropical continental storms and their comparison with those in tropical maritime regions as previously described by Atlas and Ulbrich (2006). We have divided the rains into convective, transition, and stratiform segments as observed by a disdrometer at the surface in two continental-type storms in Brazil and Arecibo, Puerto Rico. Such a division permits the characterization of the DSD, the microphysics, and the associated Z–R relations in each of the latter classes. The ultimate goal is to facilitate the selection of the most appropriate measurement algorithms for the remote measurement of rainfall and to identify their climatological behavior. The nature of the DSD is described by the parameters μ, Λ, N_0, and D_0 of a gamma distribution or the "generalized" parameter N_W. The results are displayed clearly on the μ–Λ–D_0–σ or gamma parameter diagram as developed by AU1. Our findings are as follows:

1) Each rain type has a reasonably distinctive set of D_0 values that defines the μ–Λ relation on the GPD. The larger D_0 is, the narrower is the DSD, the larger is the range of μ (the gamma shape factor), and the smaller is the range of Λ (the slope of the tail of the DSD).
2) The more liquid water that is concentrated near D_0, the narrower the DSD is and the larger μ and Λ are.
3) The D_0 found in the continental storm at Arecibo increase from about 0.5–1.5 mm (for S and T regions) to 2–3 mm in C1 and C2 convective cells; μ ranges from 0 to 15 in stratiform rain portions, but the largest values are usually due to truncation and small numbers of particles. Values of $3 < \mu < 12$ occur in the C rain regions.
4) The largest D_0 values at Arecibo and Brazil fall between 2 and 3 mm with narrow DSDs and large μ. These correspond to near-equilibrium DSDs. Such an equilibrium DSD also occurs in the maritime rains of TOGA but with smaller D_0 and thus a smaller μ and a larger Λ.
5) The general process for the formation of equilibrium DSDs is by collision, coalescence, and breakup as described by Hu and Srivastava (1995, and others referred to therein) and elaborated by Atlas and Ulbrich (2000). The drop growth is entirely in the warm phase in maritime regions and is predominantly warm in Brazil and Arecibo until the updraft extends above the 0°C level. When the rain has a large distance of fall below the 0°C level, there is sufficient time for the CCB process to operate and control the DSD regardless of the microphysics above that level.
6) Narrow equilibrium-like DSDs with large drops are characteristic of the initial convective rains. The corresponding coefficient A in $Z = AR^b$ increases with D_0 while the values of b approach unity. The A value is usually much larger and b is much smaller than most of those reported in the literature because of the failure of prior investigators to partition the rain into C, T, and S types.

7) Because the convective segment of the rain is frequently responsible for the major share of the total storm rainfall, it is important to select an appropriate Z–R relation for each portion of a storm. We suggest that this may be done by a measure (or prediction) of the updraft strength that generally controls the magnitude of D_0.
8) The differential reflectivity ZDR–Z relations for both the Brazil and Arecibo storms agree remarkably well with radar measurements in England and others in Alabama despite the much smaller samples by the JWD in comparison with the typical radar pulse volumes. The small JWD samples tend to truncate the DSD at both small and large sizes because of the greatly reduced number of such drops and thus they produce a somewhat narrower DSD than is likely to be present aloft. However, this cannot explain such a narrow DSD as that with $\mu = 6$–12.
9) ZDR depends not only upon D_0, but also on μ and $D_{\max}$. That is, the narrower the DSD is, the greater is the number of drops centered around D_0 having large ellipticity and, the larger the polarization shape effect is, the greater ZDR is. These big drops are also larger than those found in maritime storms for the same reasons.
10) The evolution of the ZDR–Z relation observed by polarimetric radar in Alabama is consistent with the time and space dependence of convective, transition, and stratiform rain, thus supporting the need for selecting algorithms suited to the rain types.
11) The N_W–D_0 pairs found here and implied in AU1 agree with the findings of distinct clusters of such pairs by Bringi et al. (2003) for maritime and continental convective rains. Agreement is improved when considering the fact that BRAL included both transition and stratiform rains in their convective storm grouping.
12) Methods for remote sensing and parameterization must partition the rainstorms into convective, transition, and stratiform segments.
13) As in all other studies based upon point DSD observations at the surface or aloft, the results presented here are subject to the caveats associated with making measurements with a real-world radar.

Acknowledgments. We greatly appreciate the continued hospitality of our home institutions and the support provided for the publication of this work. We also express our appreciation to Edwin Campos (IMF, San Jose, Costa Rica) and Monique Petitdidier (CNET-UVSQ-CNRS, Vélizy, France) for their assistance in collecting the disdrometer data in Puerto Rico. We are most grateful to Dr. Rob Cifelli for a very perceptive review that served to enhance this paper. We dedicate this paper to the many friends and colleagues who have contributed to the advances in the physics of rainfall and its measurement by radar. We particularly want to remember our deceased friends and mentors, Louis Battan, Ralph Donaldson, Herbert Ligda, Stewart Marshall, Kenneth Gunn, Walter Hitschfeld, Raymond Wexler, Frank Ludlam, Shepard Bartnoff, and Vernon Plank. Special thanks also are given to Ramesh Srivastava, Roger Lhermitte, Keith Browning, Edwin Kessler, Kenneth Hardy, Robert Meneghini, Robert Serafin, Frank Marks, Richard Carbone, and Arthur Jameson. Our many years of work in this arena have been a joy.

REFERENCES

Atlas, D., and A. C. Chmela, 1957: Physical-synoptic variations of drop-size parameters. *Proc. Sixth Weather Radar Conf.,* Boston, MA, Amer. Meteor. Soc., 21–29.

——, and C. W. Ulbrich, 1977: Path- and area-integrated rainfall measurement by microwave attenuation in the 1 to 3 cm band. *J. Appl. Meteor.,* **16,** 1322–1331.

——, and ——, 2000: An observationally based conceptual model of warm oceanic convective rain in the Tropics. *J. Appl. Meteor.,* **39,** 2165–2181.

——, and C. R. Williams, 2003: The anatomy of a continental tropical convective storm. *J. Atmos. Sci.,* **60,** 3–15.

——, and C. W. Ulbrich, 2006: Drop size spectra and integral remote sensing parameters in the transition from convective to stratiform rain. *Geophys. Res. Lett.,* **33,** L16803, doi:10.1029/2006GL026824.

——, ——, F. D. Marks Jr., E. Amitai, and C. R. Williams, 1999: Systematic variation of drop size and radar-rainfall relations. *J. Geophys. Res.,* **104,** 6155–6169.

Battan, L. J., 1973: *Radar Observation of the Atmosphere.* University of Chicago Press, 324 pp.

Brandes, E. A., G. Zhang, and J. Vivekanandan, 2003: An evaluation of a drop-distribution–based polarimetric radar rainfall estimator. *J. Appl. Meteor.,* **42,** 652–660.

Bringi, V. N., and V. Chandrasekar, 2001: *Polarimetric Doppler Weather Radar: Principles and Applications*. Cambridge University Press, 636 pp.

——, G.-J. Huang, V. Chandrasekar, and E. Gorgucci, 2002: A methodology for estimating the parameters of a gamma raindrop size distribution model from polarimetric radar data: Application to a squall-line event from the TRMM/Brazil campaign. *J. Atmos. Oceanic Technol.,* **19,** 633–645.

——, V. Chandrasekar, J. Hubbert, E. Gorgucci, W. L. Randeu, and M. Schoenhuber, 2003: Raindrop size distribution in different climatic regimes from disdrometer and dual-polarized radar analysis. *J. Atmos. Sci.,* **60,** 354–365.

Cataneo, R., and G. E. Stout, 1968: Raindrop-size distributions in humid continental climates, and associated rainfall rate-radar reflectivity relationships. *J. Appl. Meteor.,* **7,** 901–907.

Chandrasekar, V., R. Meneghini, and I. Zawadzki, 2003: Global and local precipitation measurements by radar. *Radar and Atmospheric Science: A Collection of Essays in Honor of*

David Atlas, Meteor. Monogr., No. 52, Amer. Meteor. Soc., 215–236.

Chisholm, A. J., 1973: Part I: Radar case studies and airflow models. *Alberta Hailstorms, Meteor. Monogr.,* No. 36, Amer. Meteor. Soc., 1–36.

Fujiwara, M., 1965: Raindrop-size distribution from individual storms. *J. Atmos. Sci.,* **22,** 585–591.

Halverson, J. B., T. Rickenbach, B. Roy, H. Pierce, and E. Williams, 2002: Environmental characteristics of convective systems during TRMM-LBA. *Mon. Wea. Rev.,* **130,** 1493–1509.

Hu, Z., and R. C. Srivastava, 1995: Evolution of raindrop size distribution by coalescence, breakup, and evaporation: Theory and observations. *J. Atmos. Sci.,* **52,** 1761–1783.

Illingworth, A. J., and I. J. Caylor, 1989: Polarization radar estimates of raindrop size spectra and rainfall rates. *J. Atmos. Oceanic Technol.,* **6,** 939–949.

Imai, I., M. Fujiwara, I. Imichura, and Z. Yoshihara, 1955: On the radar reflectivity and the drop-size distribution of rain. *J. Meteor. Tokyo,* **7,** 422–433.

Joss, J., and A. Waldvogel, 1967: Ein Spektrograph fur Niederschlagestrophen mit automatisher Auswerting (A spectrograph for rain drops with automatic analysis). *Pure Appl. Geophys.,* **68,** 240–246.

Marshall, J. S., and W. M. K. Palmer, 1948: The distribution of raindrops with size. *J. Meteor.,* **5,** 165–166.

Mueller, E., 1965: Radar rainfall studies. Ph.D. dissertation, University of Illinois, 93 pp.

Rosenfeld, D., and C. W. Ulbrich, 2003: Cloud microphysical properties, processes, and rainfall estimation opportunities. *Radar and Atmospheric Science: A Collection of Essays in Honor of David Atlas, Meteor. Monogr.,* No. 52, Amer. Meteor. Soc., 237–258.

Sauvageot, H., and J.-P. Lacaux, 1995: The shape of averaged drop size distributions. *J. Atmos. Sci.,* **52,** 1070–1083.

Testud, J., S. Ouray, R. A. Black, P. Amayenc, and X. Dou, 2001: The concept of "normalized" distribution to describe raindrop spectra: A tool for cloud physics and cloud remote sensing. *J. Appl. Meteor.,* **40,** 1118–1140.

Tokay, A., and D. A. Short, 1996: Evidence from tropical raindrop spectra of the origin of rain from stratiform versus convective clouds. *J. Appl. Meteor.,* **35,** 355–371.

Uijlenhoet, R., J. A. Smith, and M. Steiner, 2003: The microphysical structure of extreme precipiation as inferred from ground-based raindrop spectra. *J. Atmos. Sci.,* **60,** 1220–1238.

Ulbrich, C. W., 1983: Natural variations in the analytical form of the raindrop size distribution. *J. Climate Appl. Meteor.,* **22,** 1764–1775.

——, M. Petitdidier, and E. F. Campos, 1999: Radar properties of tropical rain found from disdrometer data at Arecibo, PR. *Proc. 29th Conf. on Radar Meteorology,* Montreal, QC, Canada, Amer. Meteor. Soc., 676–679.

Wexler, R., 1951: Theory of observation of radar storm detection. *Compendium of Meteorology,* T. F. Malone, Ed., Amer. Meteor. Soc., 1283–1289.

Zhang, G., J. Vivekanandan, E. A. Brandes, R. Meneghini, and T. Kozu, 2003: The shape–slope relation in observed gamma raindrop size distributions: Statistical error or useful information? *J. Atmos. Oceanic Technol.,* **20,** 1106–1119.

——, J. Sun, and E. A. Brandes, 2006: Improving parameterization of rain microphysics with disdrometer and radar observations. *J. Atmos. Sci.,* **63,** 1273–1290.